Catalysis Today 179 (2012) 52–60

Contents lists available at SciVerse ScienceDirect

Catalysis Today

journal homepage: www.elsevier.com/locate/cattod

Catalytic dry-reforming on Ni–zeolite supported catalyst

P. Frontera [a], A. Macario [b,*], A. Aloise [b], F. Crea [b], P.L. Antonucci [a], J.B. Nagy [b], F. Frusteri [c], G. Giordano [b]

[a] Department of Mechanics and Materials, Mediterranea University of Reggio Calabria, Reggio Calabria, Italy
[b] Department of Chemical Engineering and Materials, University of Calabria, Rende, Italy
[c] Institute, CNR-ITAE "Nicola Giordano", Via S. Lucia sopra Contesse 5, I-98126 Messina, Italy

ARTICLE INFO

Article history:
Received 31 May 2011
Received in revised form 13 July 2011
Accepted 15 July 2011
Available online 2 October 2011

Keywords:
CO_2/CH_4 reforming
Nickel catalyst
Silicalite-1
Coke formation

ABSTRACT

In the present work, the catalytic behaviour in the dry reforming of methane on Ni-based Silicalite-1 type catalyst was studied. The Silicalite-1 support has been synthesized in order to check the role of the silanol groups on the overall catalyst performance: methane and carbon dioxide conversion, hydrogen/carbon monoxide ratio and coke deposition. The population of defect groups on the Silicalite-1 surface was modified by aging of the gel, thermal treatment, ionic exchange and silylation procedure. Among these treatments, the silylation of the support surface leads to the formation of smaller and more reducible Ni-oxide species that not only improve the CH_4 and CO_2 conversion but also reduce the deactivation of the catalyst due to coke deposition and the obtained H_2/CO value is 1.04.

1. Introduction

Conversion of methane using carbon dioxide into useful products is an important research area due to the current purpose of carbon-containing emission.

The *Syngas* (CO and H_2), produced through the following catalytic processes: partial oxidation, steam reforming, dry reforming and oxy-reforming processes [1], represent a very versatile intermediate in several synthetic routes, leading to ultra-clean liquid fuels and valuable raw chemicals from alternative sources to petroleum.

In this regards, the dry reforming is an attractive way to consume CO_2, since it offers some advantages, with respect to steam reforming and the partial oxidation of methane, such as a suitable H_2/CO ratio, close to 1, for the synthesis of liquid hydrocarbons and, from an environmental point of view, it is attractive due to the reduction of carbon dioxide and methane emissions (both greenhouse effect gases) [2–4]. During the past decades, many efforts have been focused on the development of catalysts able to convert methane with high activity and, especially, with high resistance to coking. In fact, major obstacles encountered in the application of hydrocarbons reforming is the fast catalyst deactivation which is mainly due to coke accumulation and sintering of both support and active metal particles. It has been proven that supported noble metals, such as Rh, Ru, Pt, are characterized by high activity, selectivity and high resistance to coke formation [5,6]. Nevertheless, considerations of high cost and limited availability of noble metals make the development of a nickel-based catalyst more resistant to coke formation. Therefore one of the strategies to improve the coking resistance is focused on the type of the support. The effect of different supports on catalytic behaviour and coke deposition has been investigated by many research groups [7–15].

Generally speaking, suitable supports have to be resistant to temperature applied and they have to maintain the metal dispersion of the catalyst during reaction. Zeolites may have good potentiality as metal supports in the dry reforming methane, due to their interesting properties, such as high surface area, specific micropore structure, affinity to CO_2. Some type of zeolites have been tested as active metal support in dry reforming of methane and it has been observed that the nature of zeolites support influences in significant way the overall performance of the catalyst [16–20]. Moreover, in many different reactions, both activity and selectivity of zeolites can be affect by the presence of weakly acid silanol groups [21]. While, in the dry reforming of methane, a lower concentration of Lewis acid sites and the presence of a basic strength on this kind of support improve the catalyst activities and limit the coke depositions [22,23].

Among the pentasil zeolites, Silicalite-1 is an all-silica zeolite with the MFI structure with low acidity and high thermal stability and then it could be a potential support for metals to apply as catalyst in the dry reforming of methane. One of the main peculiarity of Silicalite-1 is the presence of a large amount of defects groups, up to 32 per unit cell, in the as-made form [24]. This amount can be opportunely modulated by different treatments.

In the present work we report the results, in the methane reforming reaction with CO_2, on the activity, selectivity and coke

* Corresponding author. Tel.: +39 0984496667; fax: +39 0984496655.
E-mail address: macario@unical.it (A. Macario).

0920-5861/$ – see front matter © 2011 Elsevier B.V. All rights reserved.
doi:10.1016/j.cattod.2011.07.039

Table 1
Molar gel composition, post-synthesis treatments, number of defective sites and unit cell symmetry of samples.

Sample	Molar gel composition/post-synthesis treatments	Aging of the synthesis gel	Nr. SiOH/u.c.	Symmetry of unit cell[a]
H-S1	$0.08Na_2O$–008TPABr–$1SiO_2$–$20H_2O$	Yes	5	M
H-S2	$0.08Na_2O$–0.08TPABr–$1SiO_2$–$20H_2O$	No	8	M
S-HMDS-1	Sample H-S1 after silylation procedure	–	1.3	O
S-HMDS-2	Sample H-S2 after silylation procedure	–	1.1	O

[a] M, monoclinic; O, orthorhombic.

deposition of Ni-based Silicalite-1 catalysts, obtained by different treatments in order to affect the support surface. The amount of defect groups on the Silicalite-1 surface, used as Ni-support, has been modified by different routes: aging of the gel, thermal treatment, ionic exchange and silylation procedure. The catalysts have been characterized by XRD, SEM, TPR, Thermogravimetric and NMR analyses. Particularly, the Si chemical neighbourhood of the catalyst has been studied by ^{29}Si NMR and, after the silylation treatment, by ^{13}C NMR analysis, while the nickel species obtained by catalyst reduction have been studied by TPR analysis.

2. Experimental

2.1. Catalysts preparation

All samples are prepared by hydrothermal synthesis starting from a gel with a molar composition reported in Table 1.

Particularly, 2.1 g of TPABr (98% Fluka) was dissolved in 20 g of distilled water. A solution of 0.6 g NaOH (97% Carlo Erba) in 16.2 g of distilled water was added. Finally, 6 g of the silica source, BDH (precipitated Silica gel), were added to the resulting solution under stirring for 1.5 h at room temperature. After mixing of the reagents, the gel of the H-S1 sample was aged at 303 K for 5 days and successively the reaction mixture was transferred into a Teflon lined stainless steel autoclave and heated, in static conditions, at 443 K for 24 h. For the H-S2 sample, after mixing of the reagents, the gel was directly transferred into the autoclave and heated, in static conditions, always at 443 K for 24 h.

The solid product was obtained by vacuum filtration, washed with distilled water and dried at 373 K. All samples were calcined (in air at 723 K) in order to eliminate the template.

The calcined samples were submitted to an ionic exchange, by an ammonium salt (NH_4NO_3 solution) at pH = 10.5, following strictly the procedure describe by Kitamura et al. [25], and, then, were submitted to a second thermal treatment (always at 723 K) in order to have the H-form of the catalyst (the final sample code is H-S1 and H-S2). As further post-synthesis treatment, the above mentioned and activated samples were submitted to the following silylation procedure. The samples were vacuum dried at 393 K and, then, 10 ml of toluene with hexamethyldisilazane (HMDS, as organo-silane) were added to 1 g of zeolite. The mixture was stirred for 2 h at 333 K. The HMDS/solid ratio was 0.02 for all treatments. The final solution was filtered, washed with toluene and acetone. The solid was vacuum dried at 393 K for 2 h. The silylation reaction is reported in Scheme 1.

The Ni-based catalysts were prepared by the incipient wet impregnation of the prepared supports, with a nickel content of 5 wt%. The Nickel source was the nickel nitrate hexahydrate (Sigma–Aldrich). After impregnation, the catalysts were dried overnight at 383 K and reduced at 673 K in H_2 with a flow rate of 20 cm^3 min^{-1} for 1 h.

2.2. Catalyst characterization

Phase identification of prepared catalysts was carried out recording X-ray diffractograms, using CuK_α radiation in $2\theta = 5–40^\circ$ range (Philips PW 1730/10 generator equipped with a PW 1050/70 vertical goniometer, $\lambda = 1.5404$ Å).

The morphology, crystals' dimension and habit of the crystalline phase of the products were examined on a scanning electron microscope (SEM, FEI model Inspect). N_2 adsorption–desorption isotherms were measured in order to examine the porous properties of each sample. The measurements were carried out in Micromeritics ASAP 2020 instruments. Before the analysis, all samples were pre-treated in vacuum condition at 473 K for 12 h.

Temperature programmed reduction (TPR) was carried out on Chemisorb Micromeritics 2750, to monitor the reduction of metal oxide, under a flux of 50 cc/min of H_2/Ar (10 vol.%).

The thermoanalytical measurements were performed on the automatic TG/DTA instrument (SHIMATZU) under air flow of 50 cc/min, with heating rate of 5 °C min^{-1}.

Solid state ^{29}Si NMR and ^{13}C NMR analysis was used to study the Si chemical neighbourhood of the Silicalite-1 surface before nickel deposition. NMR measurements were performed on a Bruker Avance 500 spectrometer. For ^{29}Si (99.4 MHz), at 6 μs ($\theta = \pi/6$) pulse was used with a repetition time of 40 s, while for ^{13}C (125 MHz), at 4 μs ($\theta = \pi/2$), pulse was used with a 5 ms contact time for ^{1}H–^{13}C cross polarization and a repetition time of 4 s.

For FT-IR measurements, powder samples were pressed into thin, self-supporting wafers. Spectra were collected at a resolution of 2 cm^{-1}, on a Bruker FT-IR Equinox 55 spectrophotometer equipped with a MCT detecto. Pre-treatments were carried out using a standard vacuum frame, in an IR cell equipped with KBr windows: in order to remove water and other atmospheric contaminants, wafers were outgassed for 1 h at 423 K.

High resolution transmission electron microscopy (HRTEM) investigation was carried out using a JEOL 2010F instrument equipped with a field emission gun, which allowed to achieve a point-to-point resolution of 0.19 nm and a resolution of 0.14 nm between lines, and a Philips CM12 electron microscopy provided with a high resolution camera.

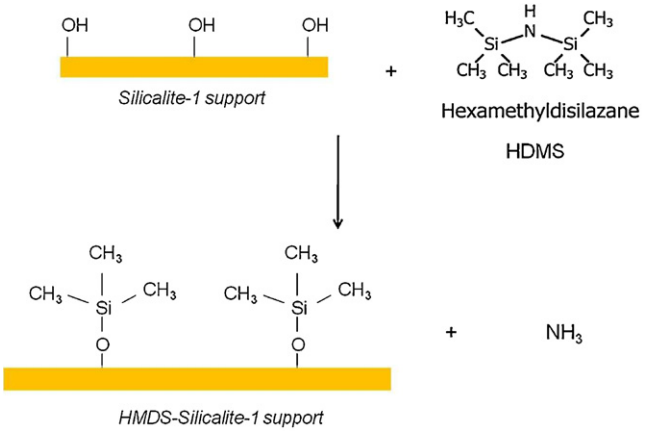

Scheme 1. Silylation reaction of the support surface.

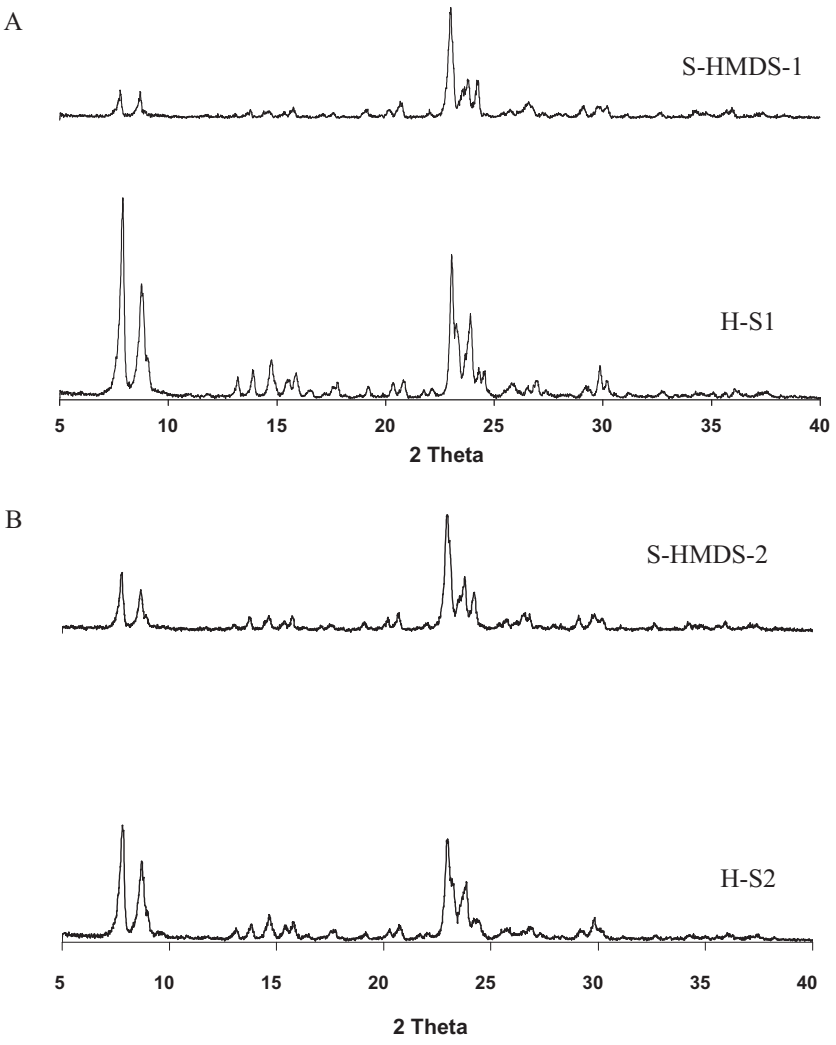

Fig. 1. XRD patterns of H-S1 and S-HMDS-1 (a) and H-S2 and S-HMDS-2 (b) samples.

2.3. Catalytic tests

The CO_2 reforming reaction of CH_4 was carried out in a continuous flow quartz tube reactor, at 1 atm and 973 K, with a constant stoichiometric mixture of CH_4 and CO_2 feed and a total flow rate of 100 ml/min. 0.2 g of catalyst were used for each catalytic test. The reaction data were monitored after 30 min on stream for 10 h. Reaction products were analyzed by on-line gas chromatograph (GC Agilent 6590) having FID and TCD detectors and four columns (Alumina, Porapak Q, Haysep, Molecular Sieves (MS 5A)), for the separation and detection of gas on outlet current on stream.

The conversion of methane and carbon dioxide in the reforming reaction were defined as follows:

$$X_{CH_4} = \frac{[CH_4]_{in} - [CH_4]_{out}}{[CH_4]_{in}} \times 100$$

$$X_{CO_2} = \frac{[CO_2]_{in} - [CO_2]_{out}}{[CO_2]_{in}} \times 100$$

where $[CH_4]_{in}$ and $[CO_2]_{in}$ are the concentrations of the reactants in the introduced feed and $[CH_4]_{out}$ and $[CO_2]_{out}$ are concentrations of the same compounds in the effluents. In addition, the molar ratio H_2:CO was obtained from the product gas composition. No by-products were observed in all experiments.

3. Results and discussion

3.1. Catalysts physical–chemical properties

By X-ray powder diffraction the typical Silicalite-1 pattern can be observed, for all synthesized catalysts. Particularly, after the first activation procedure (calcination/ionic-exchange/calcination) all samples possess a monoclinic symmetry. After the silylation procedure, the samples modify the unit cell towards an orthorhombic symmetry. In Fig. 1 the XRD patterns of the samples before and after silylation procedure have been reported. First of all we notice a crystallinity loss, but this value is very low for both samples (ca. $15 \pm 2\%$).

The main point to highlight is the unit cell evolution: from double reflection peaks, for calcined samples, to a single reflection peak at $2\theta = 24.4$ (ascribable to the orthorhombic symmetry), for silylated samples. We suggest that the $(CH_3)_3SiO$ methyl groups on the catalyst surface promote a structural rearrangement from monoclinic towards orthorhombic symmetry. In order to better investigate this aspect, the Si chemical neighbourhood has been investigated by ^{29}Si and ^{13}C NMR analysis. By the ^{29}Si NMR spectra all samples show lines in the range of -90 to -120 ppm, corresponding to different Si environments in the zeolite structure [24]. The signals above -110, can be assigned to Q^4 silicon species $[Si(OSi)_4]$ in distinct crystallographic positions of the MFI structure;

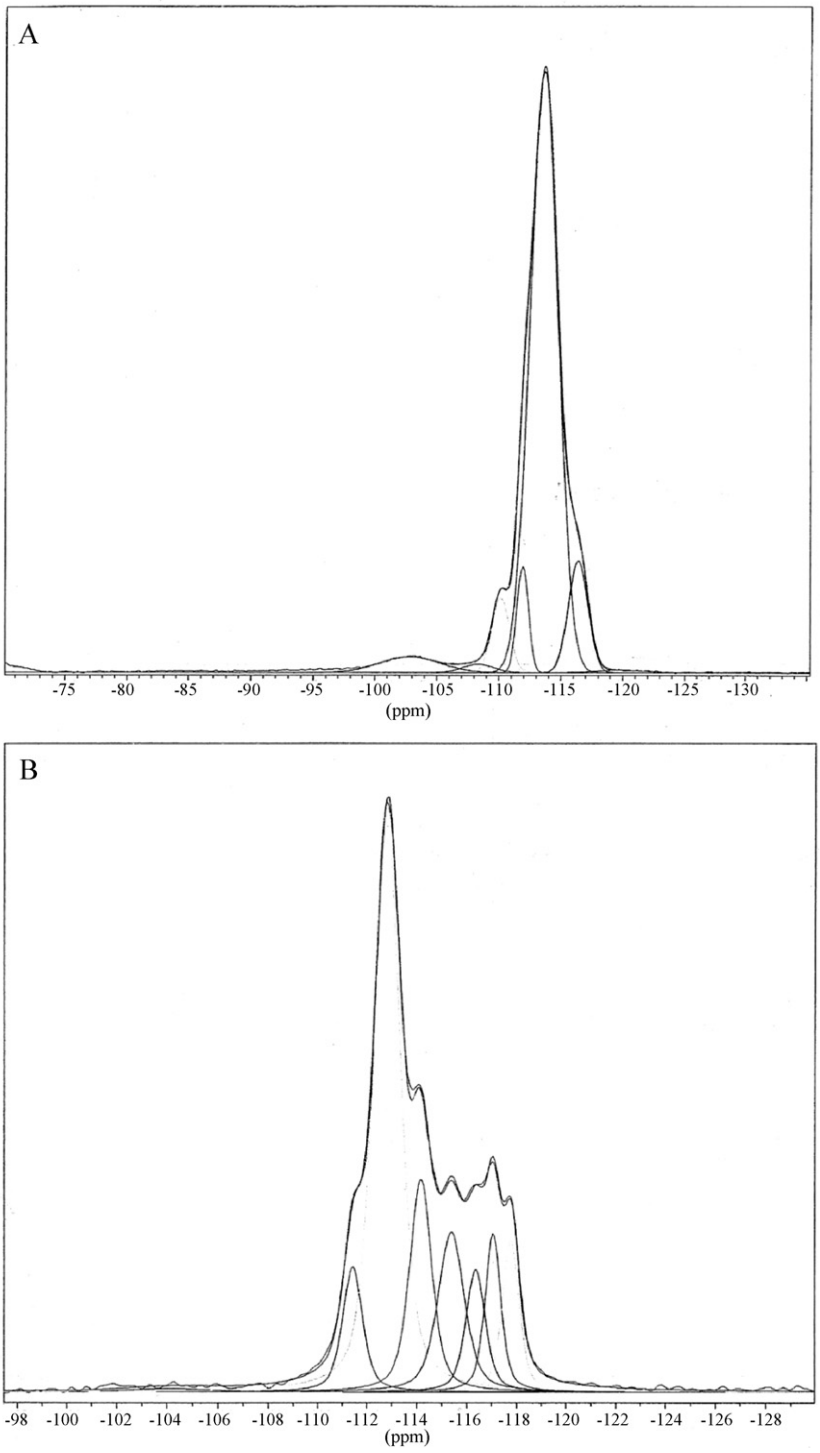

Fig. 2. ^{29}Si NMR spectra of H-S2 sample before (a) and after (b) silylation (S-HMDS-2).

the lines between −104 and −101 ppm are attributed to Q^3 silanol or single hydroxyl groups [$HOSi(OSi)_3$], while the chemical shift at −93 ppm can be attributed to Q^2 species or geminal groups [24]. This latter is absent in our samples and the silanol defective sites (Q^3) represent a small percentage of total silicon atoms present in the MFI lattice. As a matter of the fact we measured a maximum of 8 defective sites per unit cell (with respect to the 32 theoretical defective sites in the as made Silicalite-1 cell) for the sample prepared without aging of the gel, H-S2 sample (see Table 1). Differently, for the sample obtained by the aging time of the starting gel, the H-S1 sample, only five defective sites per unit cell have been detected. All these defective sites for both the samples are Q^3 species. The combination of FT-IR and NMR techniques lead to a better comprehension of the hydroxyl population in the zeolitic framework of the H-S supports. In fact, the FT-IR technique is able to identify the different isolated, nests and terminal silanols. Particularly, in the evaluation of OH stretching signals (spectra not reported) a band is detected at 3727 cm^{-1}, assigned to H-bonded silanols in terminal position, and a broad band, with maximum at ca. 3450 cm^{-1}, is ascribable to H-bonded silanols inside chains and silanols nests [26].

Table 2
Main textural properties and crystals' dimension of the prepared samples.

Sample	BET[a] (m^2/g)	V_{mic} (cc/g)	Crystals' dimension (μm)[b]
H-S1	330	0.14	1/2.5
S-HMDS-1	320	0.11	–
Ni-H-S1	300	0.13	–
Ni-S-HMDS-1	300	0.11	–
H-S2	325	0.22	10
S-HMDS-2	315	0.20	–
Ni-H-S2	300	0.15	–
Ni-S-HMDS-2	300	0.13	–

[a] Standard error ± 2%.
[b] Measured by SEM technique.

Concerning the symmetry of the unit cell, the ^{29}Si NMR spectra for H-S and S-HMD samples clearly show the difference between the silylated and not silylated structure: the intensity of lines at the chemical shifts around −114/−120 ppm is higher for the silylated sample, indicating a more rigid silicon-framework due to the presence of the organo-silane groups (see Fig. 2 for representative sample H-S2) [24]. Finally, the ^{13}C NMR spectra show a typical line at −1 ppm, for both silylated samples (S-HMDS-1 and S-HMDS-2), corresponding to the $(CH_3)_3SiO$ adsorbed species (results not shown), as a further proof that the catalyst silylation surface occurred.

As we could expect, after the silylation treatment, the amount of silanol groups (Q^3) strongly decreases: from 8 to 1.1 (of Si–OH per unit cell) for the sample S-HMDS-2, from 5 to 1.3 for sample S-HMDS-1 (see Table 1).

In Table 2 the main physical properties of the samples after silylation and metal impregnation and the crystals' dimension of the supports are reported.

The crystals' dimension of H-S supports ranges from 1 to 2.5 μm for sample prepared with aging of the synthesis gel (H-S1), while bigger crystals' dimension can be obtained for support prepared without aging of the synthesis gel (H-S2).

The loss of BET surface area of the samples, after post-synthesis treatments, has been limited. This aspect is understandable if one considers that both the groups of the organo-silane and the metal can occlude the pore mouth of the zeolite channels. For all Silicalite-1 samples, the N_2 adsorption isotherm profiles after reduction do not change significantly and all isotherms are of type I (results not shown). This indicates that in all samples the zeolite structure is preserved, as also confirmed by the stability of microporous volume value (Table 2) and by the XRD patterns reported in Fig. 3 for sample H-S2 (as representative sample) after the different treatments and activation procedures.

Finally, the morphology of the Silicalite-1 crystals are not modified by silylation, nickel impregnation and reduction, as can be observed by the SEM images reported in Fig. 4, for representative sample H-S2 after the different treatments. The rounded morphology of the crystals, in fact, can be observabed in all three SEM images.

In order to determine the behaviour of nickel metal, during the reduction treatment, and to investigate the final metal–support interactions, TPR measurements were carried out.

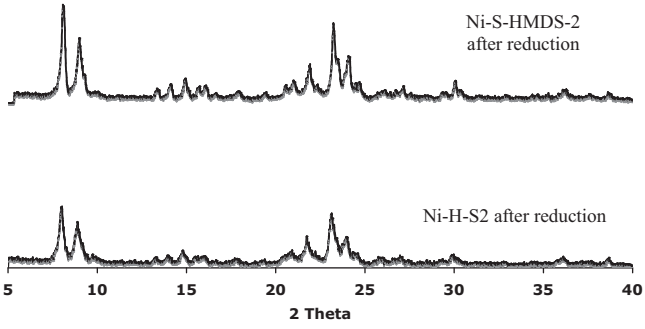

Fig. 3. XRD patterns of activated samples: Ni-H-S2 and Ni-HMDS-2 after reduction.

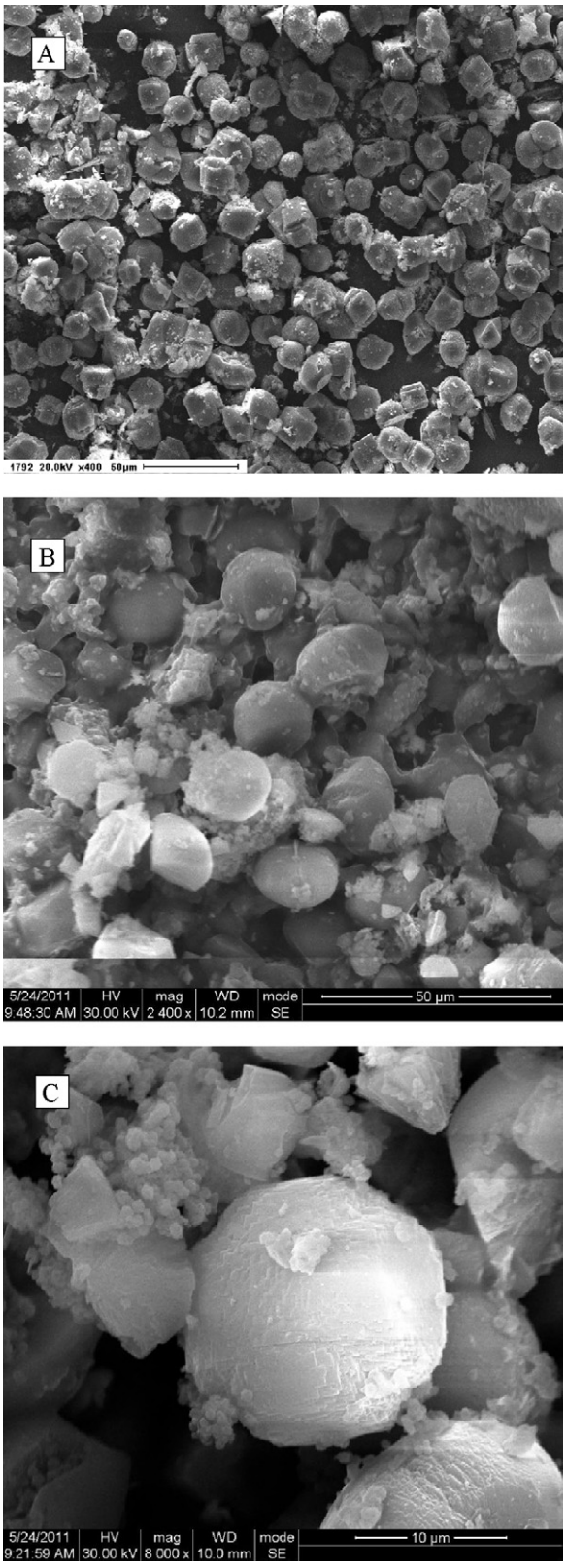

Fig. 4. SEM images of the sample H-S2 (a), Ni-H-S2 after nickel reduction (b) and Ni-S-HMDS-2 after nickel reduction.

Table 3
TPR analysis results of activated samples.

Catalyst	T_1 (K)	A_1 (%)	T_2 (K)	A_2 (%)	T_3 (K)	A_3 (%)
Ni-H-S1	573	78	611	10	803	12
Ni-H-S2	578	68	618	6	802	23
Ni-S-HMDS-1	548–568[a]	92	–	–	–	–
Ni-S-HMDS-2	583–613[a]	93	–	–	–	–

[a] The range of temperature indicates a broad peak with shoulder.

In Table 3 the reduction temperature and the relative reduction peaks areas of nickel species are reported, for each catalyst.

The reduction temperatures have been assigned as following: the first peak at lower temperature (T_1) is attributed to the reduction of NiO species segregated by weak interactions with the support or in the external surface, the second peak (T_2) is attributed to NiO-like species located inside the zeolite channels, finally, at higher temperature it is possible to observe a third peak (T_3) ascribable to the nickel particles that strongly interact with the support, probably forming nickel silicates during the activation treatment. All these peaks can be observed in the TPR profiles of the Ni metal impregnated on the not-silylated samples: Ni-H-S1 and Ni-H-S2. The species involving weak interaction represent the highest amount in both Ni-H-S1 (78%) and Ni-H-S2 (68%) samples. The species in the zeolitic channel are only 10% (for Ni-H-S1) and 6% (for Ni-H-S2). The Ni particles interacting strongly with the support are 12% for Ni-H-S1, while quite high amount is obtained for Ni-H-S2 (23%).

For the silylated samples we detected only the peak at lower temperature indicating only the presence of the NiO species, weakly bonded to the support: 92% for Ni-S-HMDS-1 and 93% for Ni-S-HMDS-2. Moreover, the TPR profiles, similar for both not-silylated catalysts, show a broad shoulder peak in the positions of lower temperature, indicating a wide typology of weak interaction between nickel oxide and support.

In the TPR profiles of the catalysts, the amount of H_2 consumption was also determined.

Table 4
CH_4 and CO_2 conversion value and H_2/CO ratio for tested samples.

Sample	CH_4 conversion (%)	CO_2 conversion (%)	H_2/CO
Ni-H-S1	62	84	1.23
Ni-H-S2	63	80	1.15
Ni-S-HMDS-1	74	83	1.04
Ni-S-HMDS-2	77	84	1.05

The highest amount of H_2 consumption for the reduction of nickel silicates was observed for sample Ni-H-S2, suggesting that the formation of nickel silicates is strongly related to the presence of defect groups.

3.2. Catalytic activity

The activity and stability of the catalysts were studied in the reaction of methane reforming by CO_2 performed at 973 K with equimolar ratio feed. In Fig. 5 are reported the CH_4 and CO_2 conversions as a function of the time on stream.

After 1 h of reaction the catalytic performance of all tested catalysts are stabilized and they remain almost constant during 10 h of reaction, indicating that no or little deactivation occurs within this period.

In Table 4 the final values of CH_4 and CO_2 conversion and H_2/CO ratio, for all catalysts tested, have been reported.

Comparing the CO_2 and CH_4 conversion value for samples Ni-H-S1 and Ni-HS-2, we observe a lower value of the CO_2 conversion for

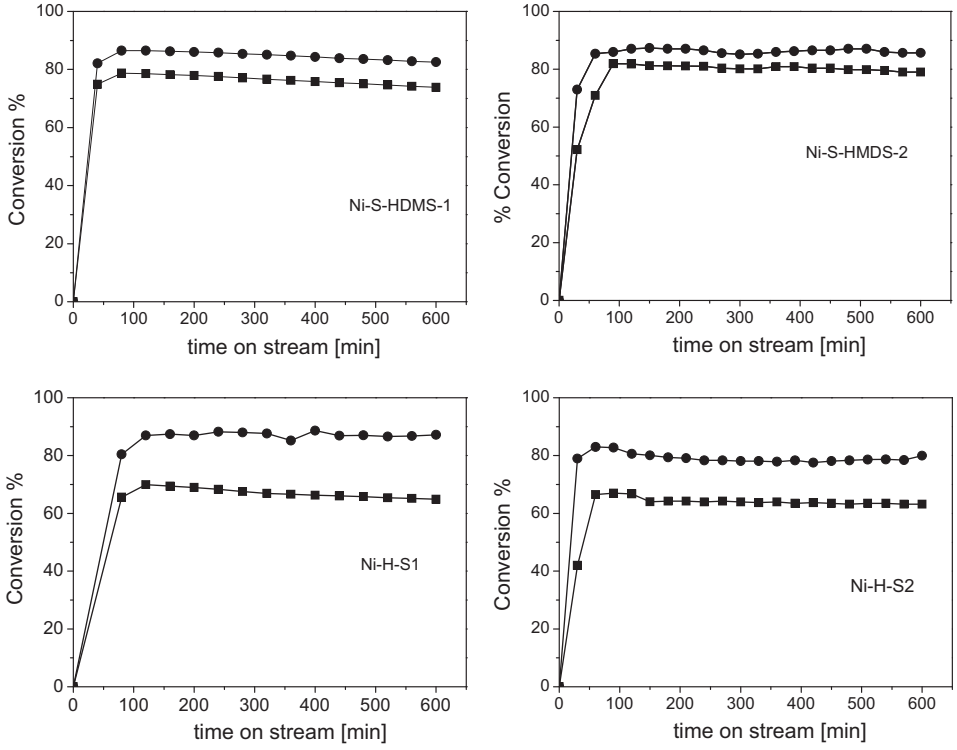

Fig. 5. The CO_2 (●) and CH_4 (■) conversion values for the catalyst tested in the dry reforming of methane.

the last sample but similar values of conversion of CH_4. By contrary, for silylated samples, the CO_2 conversion values are similar, while the CH_4 conversion obtained by Ni-S-HMDS-2 is higher than that obtained by Ni-S-HMDS-1 (77% versus 73%).

Moreover, comparing the gaps between the CO_2 and CH_4 conversion values of all samples (see Fig. 5), it is possible to observe that this gap is higher for not-silylated samples (Ni-H-S) with respect to the silylated ones (Ni-S-HMDS).

In order to explain the different values of CO_2 and CH_4 conversion of Ni supported catalyst we can be consider that the main reaction of dry reforming of methane (1) was accompanied by several secondary reactions (2)–(5), as following described:

$$CH_4 + CO_2 = 2CO + 2H_2 \quad (1)$$

$$CH_4 = C + 2H_2 \quad (2)$$

$$2CO = C + CO_2 \quad (3)$$

$$CH_4 + 3CO_2 = 4CO + 2H_2O \quad (4)$$

$$H_2O + CO = H_2 + CO_2 \quad (5)$$

In the case of the reforming of an equimolecular mixture of CH_4 and CO_2, the CH_4 and CO_2 conversions should be equal [27]. However, if the conversion of CO_2 is higher than that of CH_4 means that other reactions occur, such as the reverse water gas shift (5), as also indicated by Bradford and Vannice [28], or the CO_2 complete dissociation: $CO_2 \rightarrow CO + O$ and $CO \rightarrow C + O$, as reported by Wang and Au [29].

Moreover, if the methane conversion proceeds following reaction (1), the H_2/CO ratio has to remain near unity, while when carbon deposition occurs, this ratio is higher than 1, even if it proceeds through either CH_4 decomposition or Boudouard reaction of CO formed (3).

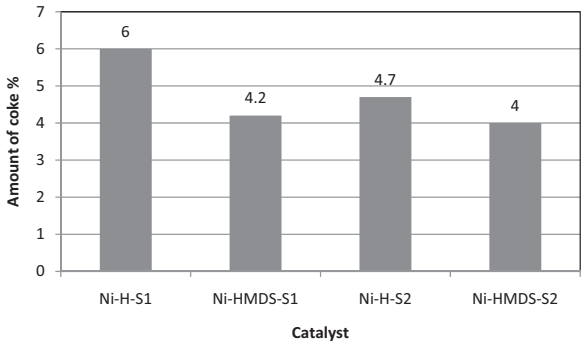

Fig. 6. The amount of coke formed of spent catalysts after catalytic testing for 10 h (reaction conditions: $T = 973$ K, $CH_4:CO_2 = 1:1$).

The H_2/CO ratio, so reported in Table 4, is nearer to unity for the silylated samples.

Differently, between the not silylated catalysts, we observe the difference in the H_2/CO ratio: for Ni-H-S1 it is greater with respect to unity (1.23) compared to the value obtained by Ni-H-S2 catalyst (1.15). This is in agreement with a lower value of CO_2 conversion for Ni-H-S2.

3.3. Carbon deposition on spent catalysts

It is generally known that the coke formation in the CO_2 reforming of CH_4 causes the catalyst deactivation. Thermogravimetric analysis (TGA) was employed to estimate the amount of carbon

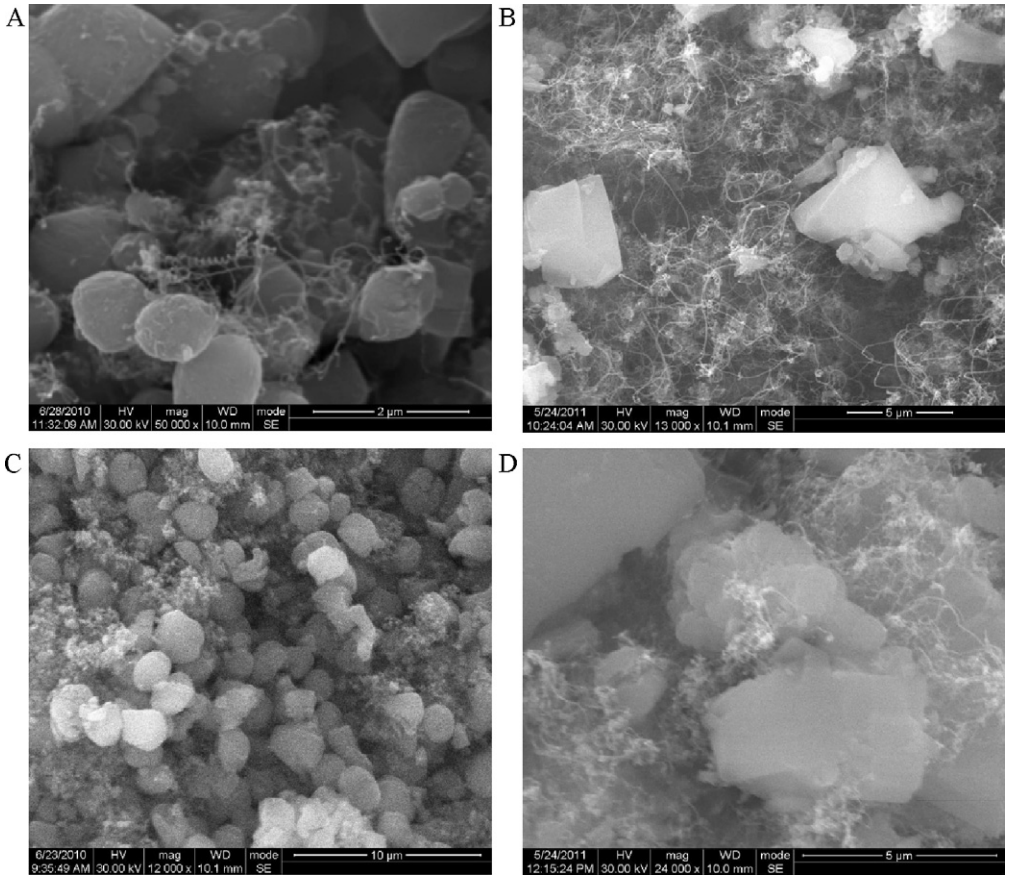

Fig. 7. SEM micrographs of spent catalysts: (A) sample Ni-H-S1, (B) sample Ni-H-S2, (C) Ni-S-HMDS-1, (D) Ni-S-HMDS-2.

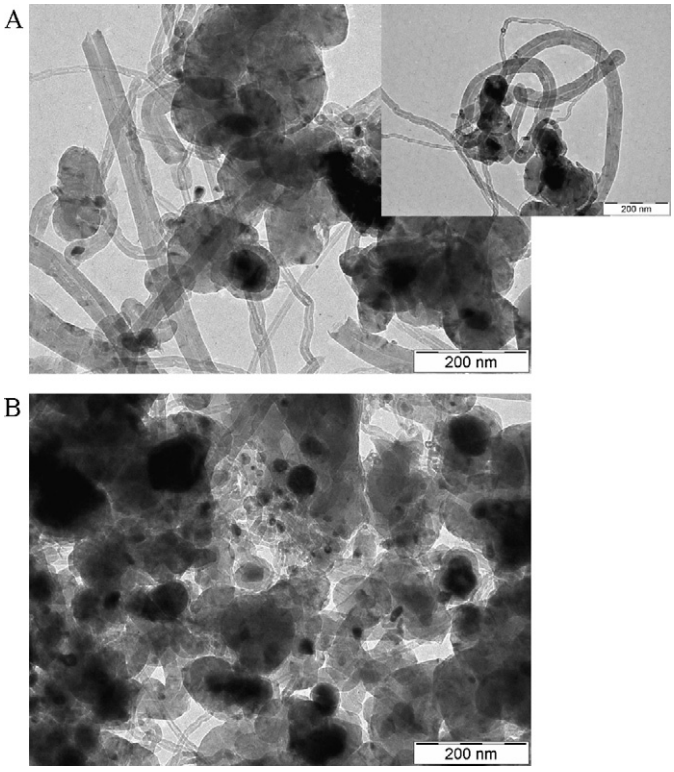

Fig. 8. TEM images of spent catalyst (A) sample Ni-H-S1, (B) Ni-S-HMDS-1.

deposition. Fig. 6 shows the amount of coke formation on the different spent catalysts. The results show clearly that the carbon deposition on spent Ni-HMDS-1 and Ni-HMDS-2 catalysts were lower than those on Ni-H-S1 and Ni-H-S2.

For samples Ni-S-HMDS-1 and Ni-S-HMDS-2 the coke deposition follows a similar trend, also in agreement with the conversion value of CO_2 and CH_4 obtained for these two catalysts.

By contrary, for the not-silylated catalysts, Ni-H-S1 and Ni-H-S2, the lower amount of coke deposition obtained for Ni-HS-2 is probably due to the different amount of nickel silicates species identified by TPR analysis for both samples. In fact, the area of the last peak which identifies the nickel silicate species (see Table 3) is twice as high for Ni-HS-2 catalyst with respect to the Ni-HS-1 sample.

Moreover, as also reported by Choi and Lee [30] for nickel on silica surface, the presence of nickel silicate species contributes to a slow deactivation. Based on this observation, it is possible to suggest that the finely dispersed nickel species on the surface with higher concentration of defect groups show a stronger metal support interaction and lead to formation of the nickel silicate species, and thus resulting in a higher resistance to deactivation.

The different behaviours are also qualitatively observed by SEM analysis. In Fig. 7 it is possible to highlight in the spent catalyst the greater presence of filamentous coke in the not silylated support samples (Ni-H-S1 and Ni-H-S2) instead of spongy agglomerates more detected on the silylated supports (Ni-S-HMDS-1, Ni-S-HMDS-2).

The difference between the two carbon forms observed on spent catalyst (filamentous and spongy agglomerates) has been also suggested by the position of the exothermic peaks of carbon combustion, detected by DTA analysis. Particularly, for not silylated samples (containing mainly filamentous coke) the temperature of combustion of structured coke is shifted to higher temperature, with respect to the combustion peak for spongy agglomerates coke deposited on silylated samples: from 850 K for sample Ni-H-S1, to 905 K for sample Ni-S-HMDS-1 (as representative samples).

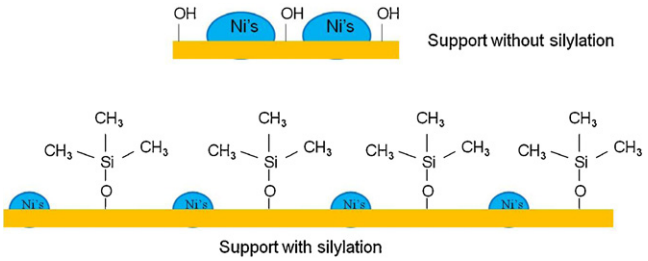

Scheme 2. Proposed mechanism of Ni deposition on the silylated support surface.

This trend it also confirmed by TEM analysis showed in Fig. 8. In sample Ni-H-S1 the coke deposit mostly consists of whisker carbon species (Fig. 8A). TEM image of the Ni-HMDS-1 highlights the change in the morphology of carbon formed, in fact, few carbon whiskers are detected and the deposits exhibit a shell-like morphology.

Hence the silylation procedure of support before the nickel impregnation determines different types of carbon deposition on Ni-catalysts.

The carbon formation of whisker type on Ni catalyst needs an ensemble of minimum 7 Ni atoms, formed by particles larger than 5 nm. Moreover, in these particles the C/Ni's ratio must be between 10 and 20 [31]. The presence of organo-silanes on the support surface during the Ni impregnation avoids the formation of large Ni agglomerates, and favours a distribution of smaller and more reducible Ni-oxide species, as proposed in Scheme 2.

4. Conclusion

In this study the influences of the external support surface on the activity of the metal catalytic sites of a Ni-based catalyst, used in the dry reforming of methane, has been correlated to the presence of the silanol defect groups on the support surface.

High amount of silanol groups on the Silicalite-1 support surface allows to obtain, during the metal activation, high amount of nickel silicate species. This high amount preserves the catalyst from high coke deposition but the H_2/CO ratio is higher than unity.

Substituting the OH groups of the support with larger organosilane groups, before the nickel impregnation, the formation of high reducible nickel oxide species occurs. This kind of catalytic sites improves the overall catalytic performance of the Ni-based catalyst in the dry reforming of methane: higher CH_4 and CO_2 conversion, H_2/CO ratio nearer to unity and lower carbon deposition have been obtained for Ni supported catalyst on silylated Silicalite-1 surface.

References

[1] T.V. Choudhary, V.R. Choudhary, Angew. Chem. Int. Ed. 47 (2008) 1828–1847.
[2] J.M. Fox III, Catal. Rev. Sci. Eng. 35 (2) (1993) 169–212.
[3] J.R. Rostrup-Nielsen, J.H. Bak-Hansen, J. Catal. 144 (1993) 38–49.
[4] A.T. Ashcroft, A.K. Cheetham, M.L.H. Green, P.D.F. Vernon, Nature 352 (1991) 225–226.
[5] J.R. Rostrup-Nielsen, in: J. Anderson, M. Boudart (Eds.), Catalysis Science and Technology, vol. 5, Springer, New York, 1984.
[6] J.S. Chang, S.E. Park, H. Chon, Appl. Catal. A: Gen. 145 (1996) 111–124.
[7] T. Horiuchi, K. Sakuma, T. Fukui, Y. Kubo, T. Osaki, T. Mori, Appl. Catal. A 144 (1996) 111–120.
[8] X.E. Verykios, Int. J. Hydrogen Energy 28 (2003) 1045–1063.
[9] E. Ruckenstein, Y.H. Hu, Appl. Catal. A 133 (1995) 149–161.
[10] Z. Zhang, X.E. Verykios, Catal. Today 21 (1994) 589–595.
[11] Y. Schuurman, C. Marquez-Alvarez, V.C.H. Kroll, C. Mirodatos, Catal. Today 46 (1998) 185–192.
[12] F. Pompeo, N.N. Nichio, O.A. Ferretti, D. Resasco, Int. J. Hydrogen Energy 30 (2005) 1399–1405.
[13] B. Pavelec, S. Damyanova, K. Arishtirova, J.L. Fierro, L. Petrov, Appl. Catal. A: Gen. 30 (2007) 188–201.
[14] J.R. Rostrup-Nielsen, J. Sehested, J.K. Nørskov, Adv. Catal. 47 (2002) 65–139.
[15] J.R.H. Ross, Catal. Today 100 (2005) 151–158.

[16] A. Kaengsilalai, A. Luengnaruemitchai, S. Jitkarnka, S. Wongkasemjit, J. Power Sources 165 (2007) 347–352.
[17] P. Frontera, A. Aloise, A. Macario, P.L. Antonucci, F. Crea, G. Giordano, J.B. Nagy, Top. Catal. 53 (2010) 265–272.
[18] W. Nimwattanakul, A. Luengnaruemitchai, S. Jitkarnka, Int. J. Hydrogen Energy 31 (2006) 93–100.
[19] K. Wang, X. Li, S. Ji, S. Sun, D. Ding, C. Li, Stud. Surf. Sci. Catal. 167 (2007) 367–372.
[20] J.S. Chang, S.E. Park, J.W. Yoo, J.N. Park, J. Catal. 195 (2000) 1–11.
[21] B. Bonelli, L. Forni, A. Aloise, J.B. Nagy, G. Fornasari, E. Garrone, A. Gedeon, G. Giordano, F. Trifirò, Microporous Mesoporous Mater. 101 (2007) 153–160.
[22] J.A. Montoya, E. Romero-Pascual, C. Gimon, P. Del Angel, A. Monzón, Catal. Today 63 (2000) 71–85.
[23] D. Halliche, O. Cherifi, Y.B. Taarit, A. Auroux, Kinet. Catal. 49 (2008) 667–672.
[24] G. Engelhardt, D. Michel, High-Resolution Solid-State NMR of Silicates and Zeolites, Wiley & Sons Ltd., New York, 1987.
[25] N. Kitamura, H. Hichihashi, I. Tojima, US Patent 5 212 302, 1993.
[26] S. Bordiga, P. Ugliengo, A. Damin, C. Lamberti, G. Spoto, A. Zecchina, G. Spanò, R. Buzzoni, L. Dalloro, F. Rigetti, Top. Catal. 15 (2001) 43–52.
[27] J.Z. Luo, L.Z. Gao, C.F. Ng, C.T. Au, Catal. Lett. 62 (1999) 153–158.
[28] M.C.J. Bradford, M.A. Vannice, Catal. Rev. Sci. Eng. 41 (1999) 1–42.
[29] H.Y. Wang, C.T. Au, Appl. Catal. A 155 (1997) 239–252.
[30] Y.H. Choi, W.Y. Lee, Catal. Lett. 67 (2000) 155–161.
[31] M.C. Demicheli, D. Duprez, J. Barbier, E.N. Ponzi, O.A. Ferretti, J. Catal. 145 (1994) 437–449.